Surface rupture during the 2010 M_w 7.1 Darfield (Canterbury) earthquake: Implications for fault rupture dynamics and seismic-hazard analysis

M. Quigley[1], R. Van Dissen[2], N. Litchfield[2], P. Villamor[2], B. Duffy[1], D. Barrell[3], K. Furlong[4], T. Stahl[1], E. Bilderback[1], and D. Noble[1]
[1]Department of Geological Sciences, University of Canterbury, 8140 Christchurch, New Zealand
[2]GNS Science, Lower Hutt 5040, New Zealand
[3]GNS Science, Dunedin 9016, New Zealand
[4]Department of Geosciences, Pennsylvania State University, University Park, Pennsylvania 16802, USA

ABSTRACT

The September 2010 M_w 7.1 Darfield (Canterbury) earthquake in New Zealand is one of the best-recorded earthquakes of this magnitude. The earthquake occurred on a previously unidentified fault system and generated a 29.5 ± 0.5-km-long surface rupture across a low-relief agricultural landscape. High-accuracy measurements of coseismic displacements were obtained at over 100 localities along the Greendale fault. Maximum net displacement (D_{max}) (5.3 ± 0.5 m) and average net displacement (D_{avg}) (2.5 ± 0.1 m) are anomalously large for an earthquake of this M_w. D_{max} / surface rupture length (*SRL*) and D_{avg}/*SRL* ratios are among the largest ever recorded for a continental strike-slip earthquake. "Geologically derived" estimates of moment magnitude (M_w^G) are less than the seismologically derived M_w, derived using widely employed *SRL*-M_w scaling regressions. M_w^G is greater than M_w using D_{max}- and D_{avg}-M_w regressions. The "geologically derived" static stress drop of 13.9 ± 3.7 MPa provides a context with which to compare this earthquake rupture to interplate and intraplate ruptures of similar M_w. This data set provides fundamental information on fault rupture processes relevant to seismic-hazard modeling in this region and analogous settings globally.

INTRODUCTION

The documentation of earthquake-induced surface ruptures (e.g., Clark, 1972) is a fundamental component of fault scaling relationships used for seismic-hazard analysis, engineering design criteria, and studies of fault rupture dynamics (e.g., Wells and Coppersmith, 1994; Wesnousky, 2008). Fault rupture data also enable estimation of static stress changes during earthquakes that provide insight into fault strength (e.g., Griffith et al., 2009) and the modeling of past and future earthquakes (e.g., Price and Bürgmann, 2002). Considerable variability exists in the surface rupture length (*SRL*) of moderately sized (i.e., M_w 7.0 ± 0.1) historical continental earthquakes, from nil (e.g., the 2010 M_w 7.0 Haiti earthquake; Prentice et al., 2010) to many tens of kilometers (e.g., 60 km *SRL* for the 1940 M_w 7.0 Imperial Valley, California, quake; Trifunac and Brune, 1970), highlighting the importance of combining geologic with seismologic and geodetic data sets in rupture analysis. Short or absent surface ruptures for continental earthquakes may reflect a concentration of coseismic slip at depth (Wesnousky, 2008) and/or complex ruptures on several faults without surface breaks (e.g., Hayes et al., 2010).

The 2010 M_w 7.1 Darfield (Canterbury) earthquake, henceforth referred to as the "Darfield" earthquake, occurred at 04:35 on 4 September 2010 New Zealand local time (16:35, 3 September UTC), with an epicenter located ~44 km west of the Christchurch central business district and a hypocentral depth of ~10.7 km (Fig. 1B) (Gledhill et al., 2011). (The Darfield earthquake was followed by a pronounced aftershock sequence, termed the "Canterbury earthquake sequence," including a M_w 6.2 aftershock located 10 km southeast of the Christchurch central business district at 12:51 on 22 February local time that caused 182 fatalities and an estimated U.S. \$10 billion worth of damage [see the GSA Data Repository[1], and Gledhill et al., 2011].)

The earthquake was recorded by dense networks of broadband and strong-motion seismometers (Gledhill et al., 2011), and ground displacements were obtained from global positioning system (GPS) surveying and interferometric synthetic aperture radar (InSAR) (Beavan et al., 2010). Rapidly deployed field teams identified and began to map the surface fault rupture trace only hours after the earthquake (Quigley et al., 2010). The rupture occurred across a relatively flat, post–last glacial alluvial plain (Forsyth et al., 2008) with an extensive agricultural framework. This provided >100 displaced markers (Fig. 2) that could be measured to determine *SRL* and coseismic displacements.

In this paper, we use real-time kinematic (RTK) and differential (D) GPS surveying, tape measurements, and airborne light detecting and ranging (LiDAR) to document the Greendale fault (GF) surface rupture during the 2010 Darfield earthquake. The rapid collection of field surface rupture data provides an opportunity to reduce the uncertainties in the displacement measurements and geometrical characteristics of earthquake surface rupture. We compare these data with data from other historical surface ruptures associated with earthquakes of similar M_w, and discuss the broader implications for fault behavior, M_w-displacement-*SRL* scaling relationships, and seismic-hazard analysis.

GEOLOGIC SETTING

New Zealand occupies the boundary zone between the Pacific and Australian plates, which converge obliquely at rates of 39–50 mm yr^{-1} (DeMets et al., 2010) (Fig. 1A). In the central South Island, continent-continent collision is characterized by dextral transpression across a series of predominantly NNE- to east-striking active faults throughout the Southern Alps, the Canterbury Plains, and offshore (Pettinga et al., 2001) (Figs. 1A and 1B). Geodetic data indicate ~2 mm yr^{-1} of contraction oriented at 277° ± 8° across the 125-km-wide Canterbury Plains block with a western boundary defined by the Porter's Pass–Amberley fault zone (PPAFZ; Fig. 1B) (Wallace et al., 2007). The stress field in the area of the Darfield earthquake is best characterized by a subhorizontal maximum compressive stress (s_1) trending ~115° ± 5° (Fig. 2) (Sibson et al., 2011). Structures in the Canterbury Plains block (Fig. 1B), such as the fault underlying the Hororata anticline (Jongens et al., 1999) and the Springfield fault (Forsyth et al., 2008), deform the post–last glacial alluvial outwash surface, implying Late Pleistocene or Holocene deformation. No evidence for prior surface-rupturing earthquakes was observed in the vicinity of the GF.

[1]GSA Data Repository item 2012015, derivation of surface rupture length, displacement, magnitude, and stress drop for the Greendale fault rupture, is available online at www.geosociety.org/pubs/ft2012.htm, or on request from editing@geosociety.org or Documents Secretary, GSA, P.O. Box 9140, Boulder, CO 80301, USA.

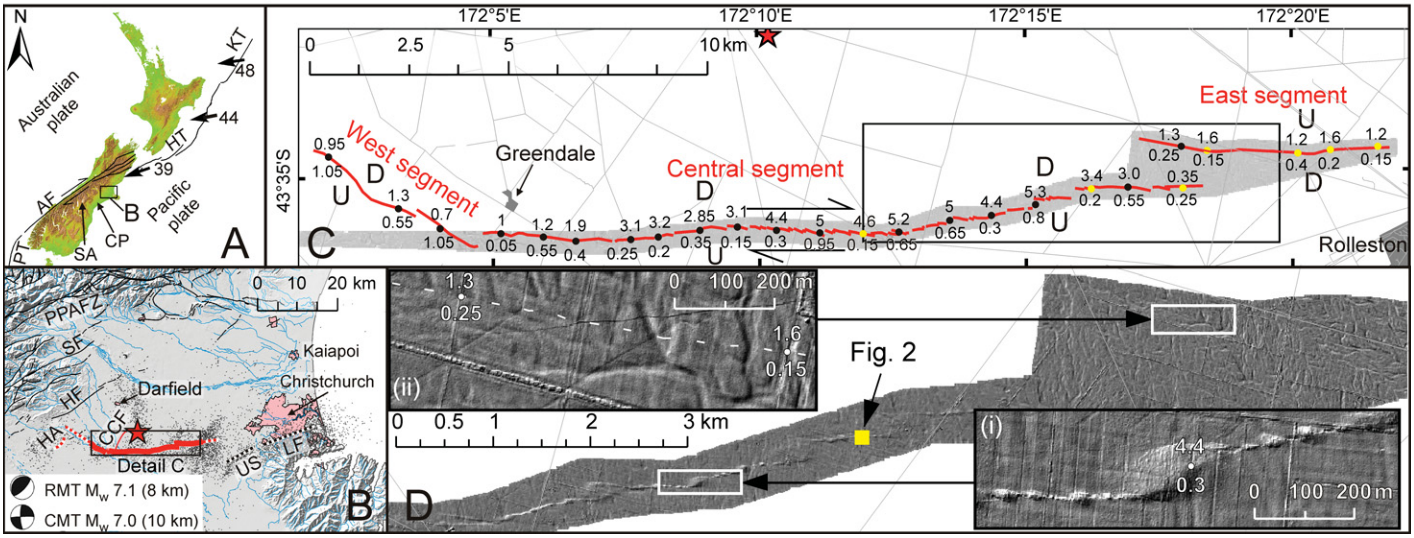

Figure 1. A: New Zealand plate boundary setting and DeMets et al. (2010) relative motion vectors (mm yr^{-1}) between the Australian and Pacific plates. Canterbury Plains (CP) form the low relief (green) east of the Southern Alps (SA) in the central South Island. PT—Puysegur Trench; AF—Alpine fault; HT—Hikurangi Trough; KT—Kermadec Trough. B: Location of the Greendale fault in Canterbury. Red star is Darfield earthquake epicenter. Moment tensor solutions and depths after Gledhill et al. (2011). RMT—regional moment tensor; CMT—centroid moment tensor. Greendale fault surface rupture shown bold solid red, blind ruptures shown dotted red. CCF—Charing Cross fault; HA—Hororata anticline. M ≥ 3 aftershocks shown up to 17 May 2011. Dotted black structures are Lyttleton fault (LF, aftershock rupture 22 February 2011) and an unnamed structure (US). All other structures (fine black lines) are from Forsyth et al. (2008). HF—Hororata fault; SF—Springfield fault; PPAFZ—Porter's Pass–Amberley fault zone. C: Detailed fault trace map. U and D are relative up and down sides. Selected offset measurements shown along surface rupture. Top number is dextral offset, bottom number is vertical offset. Yellow markers up to north, black markers up to south. Light gray polygon shows extent of LiDAR swath. D: LiDAR panel with details showing (i) the excellent imaging of the en echelon structures of the central trace and (ii) poor imaging of the trace (dashed white line) toward the eastern rupture terminus.

SURFACE RUPTURE CHARACTERISTICS

The GF surface rupture was mapped in detail and >100 horizontal (HD), vertical (VD), and net displacements (*D*) were obtained by measuring offsets of formerly linear features. These include roads, fences, hedgerows, crop and tree lines, irrigation channels, tire tracks, and power lines. Methodological details are provided in the Data Repository.

The mapped surface rupture is 29.5 ± 0.5 km long. Along the eastern ~8 km of the rupture, deformation is expressed as subtle horizontal flexure with no discrete ruptures, fissures, or vertical scarps, and thus was recognized by mapping the deformation of previously straight, well-defined features such as roads and fences. The east and west rupture tips were located by mapping where such features were no longer deformed (see the Data Repository). The uncertainty in fault tip location is ±100 m at the east tip and ±450 m at the west tip. We estimate that no more than ~70% of the total *SRL* (forthwith "SRL_{min}"; ~20.6 km) would have been mapped without reference to these man-made features.

The gross fault rupture morphology is that of two definable east-west–striking segments (eastern and central segments) and a NW-striking segment (western segment) collectively referred to as the GF (Figs. 1C and 3). The east and central fault segments are defined as a series of east-west–striking, left-stepping en echelon surface traces (Figs. 1C and 1D). The widest step-over (~950 ± 50 m) measured perpendicular to the average strike of adjacent rupture traces occurs between the east and central segments. The next widest step-over (~500 m) separates the west and central segments. There are another ~20 step-overs between 75 and 250 m wide. The surface rupture zone contains a multitude of features commonly observed within earthquake ruptures dominated by simple shear (e.g., Terres and Sylvester, 1981). These include approximately east-west–striking dextral faults, WNW-oriented synthetic Riedel (R) dextral shear fractures, approximately NNW-oriented antithetic (R′) sinistral shear fractures, approximately NW-SE–oriented tension fractures, approximately NE-SW–oriented folds and thrust/reverse faults, and decimeter-amplitude vertical flexure and bulging (Figs. 1D and 2). Pop-up structures formed at most of the restraining left-steps with amplitudes up to ~1 m (Fig. 1D).

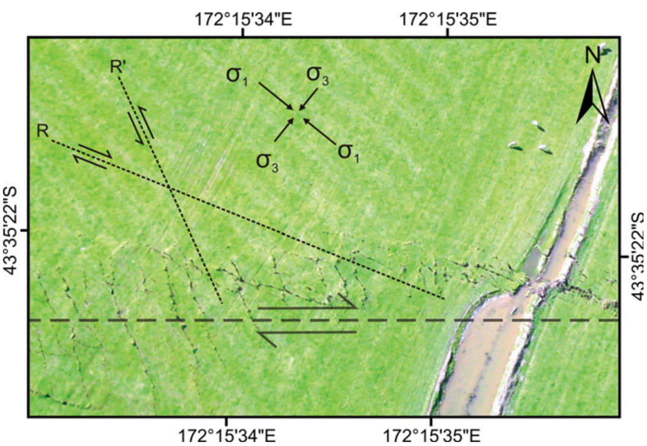

Figure 2. Rupture morphology showing dextral fault trace (horizontal dashed line) and interpreted structures and principal stress orientations. R shears are dextral, R′ shears are sinistral. Canal was not completely straight prior to rupture, pond to south was pre-existing. Total dextral displacement at site is 3.5 m. For location of photo, see Figure 1D.

The distribution of HD and *D* is approximately symmetric along the fault (Figs. 3A and 3C), with ~6 km at either end of the fault where *D* is ≤1.5 m, and an ~8-km-long central section where *D* is ≥4 m. HD and *D* are distributed across a 30–300-m-wide deformation zone, largely as horizontal flexural folding. On average, 50% of *D* occurs over 40% of the total width of the deformation zone. Discrete faults were

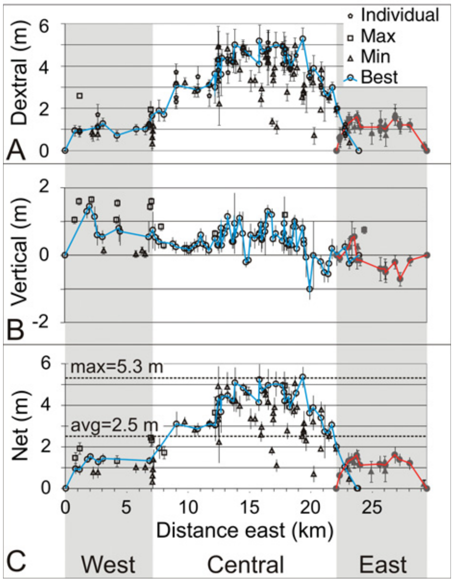

Figure 3. Displacement plots showing (A) dextral, (B) vertical (positive values are south-side-up, negative are south-side-down), and (C) net displacements including maximum and average values. Open symbols—west/central segments; filled gray symbols—eastern segment. Several individual dextral displacement markers were measured per site (e.g., fence, road, and ditch). Depending on feature orientation, continuity, and original straightness, measured displacements were classified as minimum (min), maximum (max), and best estimates. Displacement on east segment shown with filled gray circles and red line. Error bars define 2σ limits.

generally not observed where D is ≤1.5 m and typically account for only a minor component of D. In the east part of the central fault segment is an ~5-km-long sector where D is ≥5 m. This sector includes D_{max} of 5.3 ± 0.5 m and HD_{max} of 5.2 ± 0.2 m (all displacement errors reported at 2σ; i.e., 95% confidence) (Figs. 3A and 3C). The maximum VD (1.45 ± 0.2 m) occurs ~2 km from the west end of the fault in the western rupture segment (Fig. 3B). VD across the full length of the surface rupture deformation zone is typically <0.75 m (Fig. 3B). VD is generally south-side-up, though the east ~6 km of rupture is north-side-up. VD increases locally to ~1–1.5 m at major restraining and releasing bends. Best-fit curves through the D data yield a best-fit D_{avg} of 2.5 ± 0.1 m (Fig. 3C; see the Data Repository). The average strike-slip to dip-slip ratio is ~5:1.

DERIVATION OF M_W^G AND $\Delta\sigma^G$ USING GEOLOGIC DATA

To investigate whether we would have accurately estimated the M_w potential of the GF from surface rupture characteristics alone, as would be employed in paleoseismic analysis, we used the SRL, D_{max}, and D_{avg} versus M_w global strike-slip earthquake regressions of Wells and Coppersmith ("WC"; 1994) and Wesnousky ("Wky"; 2008) (see the Data Repository for equations) to derive "geologic" estimates of moment magnitude (M_w^G). Using WC, we find M_w^G = 6.8 ± 0.2 for SRL, M_w^G = 6.6 ± 0.2 for SRL_{min}, M_w^G = 7.4 ± 0.1 for D_{max}, and M_w^G = 7.4 ± 0.1 for D_{avg}. Using Wky, we find M_w^G = 6.8 for SRL and M_w^G = 6.7 for SRL_{min}. Using Hanks and Kanamori ("HK"; 1979) (see the Data Repository) and subsurface fault length $L = (4/3)SRL$ = 39.3 km (within error of geodetically derived L from Beavan et al., 2010), crustal rigidity $\mu = 3 \times 10^{11}$ dyne/cm^2, and rupture width W = 12 ± 2 km (Gledhill et al., 2011), we find M_w^G = 7.0 ± 0.1 for SRL and 6.9 ± 0.05 for SRL_{min}. Using Berryman et al. ("B"; 2002) (see the Data Repository) we find M_w^G = 7.0 ± 0.1 for $L = (4/3)SRL$ and 6.9 ± 0.1 for $L = (4/3)SRL_{min}$. Uncertainties in the conversion of SRL to L broaden the error range in M_w estimates.

Beavan et al. (2010) calculated the GF-only M_w = 7.0 using a GPS and InSAR-derived fault source model. WC and Wky SRL-based regressions thus underestimate the Darfield earthquake M_w and are at the low end, albeit within error, of the GF-only M_w. WC and Wky SRL_{min} regressions significantly underestimate M_w. WC D_{max} and D_{avg} regressions significantly overestimate M_w. HK and B equations provide SRL-based estimates within error of M_w and SRL_{min}-based estimates below M_w and within error of the GF-only M_w.

Using the surface rupture data and elliptical fault model equation of Madariaga (1977; see the Data Repository), we calculate a "geologic" estimate of coseismic static stress drop on the GF rupture ($\Delta\sigma^G$) of 13.9 ± 3.7 MPa.

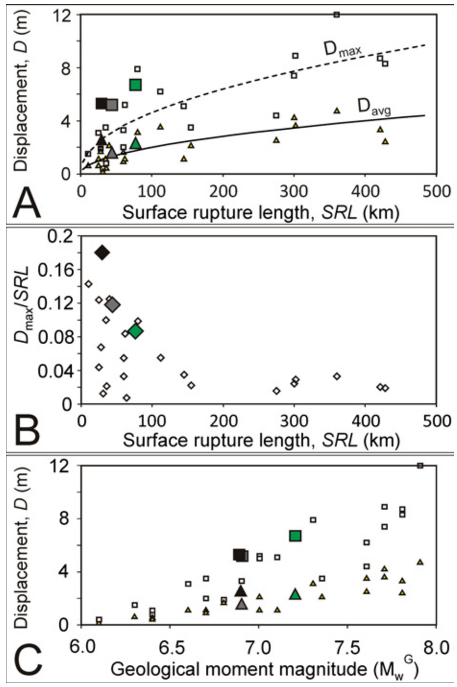

Figure 4. Rupture scaling relationships for large strike-slip earthquakes (open symbols), specifically including the Darfield (black symbols), Landers (green symbols), and Hector Mine earthquakes (gray symbols). A: D_{max} (squares) and D_{avg} (triangles) plotted against surface rupture length (SRL) and power law regressions from Wesnousky (2008). D_{avg} for the Darfield earthquake plots on the D_{max} trend. B: Ratio D_{max}/SRL plotted against SRL for the same earthquakes. The ratio for the Greendale fault is 25% greater than any other historic rupture. C: D_{max} and D_{avg} versus geological moment magnitude (M_w^G). Greendale fault data plot above the trend. Data and plots modified from Wesnousky (2008).

DISCUSSION

Our high-resolution documentation of the GF surface rupture provides an exceptional opportunity to investigate earthquake behavior in a relatively low-strain-rate region of an active plate boundary zone. Several interesting aspects of the GF rupture are evident when surface rupture attributes are compared to those of other historical earthquakes (Fig. 4). GF D_{max}:SRL, D_{avg}:SRL, D_{max}:M_w^G, and D_{avg}:M_w^G ratios are the highest of any fault rupture in this data set (Fig. 4). This implies that (1) coseismic displacement was exceptionally high for the fault length, (2) maximum fault slip distribution was concentrated at shallow depths, and/or (3) the precision with which this rupture is measured is higher than is typically achievable for most earthquakes. Each of these possibilities has merit. In support of 1 and/or 2, GF D_{avg} and D_{max} are 2.0–2.3 times (using GF SRL) and 1.8–2.0 times (using GF L) the predicted values obtained from SRL versus D_{avg} or D_{max} regressions for global strike-slip earthquakes (e.g., "power-law" from Wesnousky, 2008). Preliminary strong-motion seismic-source models support hypothesis 2 in that modeled maximum GF slip is concentrated at shallow (≤3 km) depths (Holden et al., 2011). With respect to 3, the ability to document rupture endpoints and displacements using agricultural features gives high confidence in the SRL and D data we present. An absence of these features would have reduced our mapped SRL by ~30% and D by an unquantified amount due to the typical distribution of D across ~50–100-m-wide deformation zones that involve only a minor component of offset on discrete faults (Fig. 1D; see the Data Repository). We suspect that SRL and D documentation prior to the development of modern surveying techniques (e.g., RTK GPS, InSAR, LiDAR) and in areas of remote and/or rugged topography, areas similarly underlain by poorly consolidated alluvial deposits that tend to distribute deformation, and/or areas where linear markers are not abundant, may not have achieved the same resolution that was possible in this instance.

Commonly used empirical relationships yield GF estimates of $M_w^G \le M_w$ using *SRL* and $M_w^G >> M_w$ using D_{avg} and D_{max}. This highlights the challenges of using *SRL* and *D* data obtained in paleoseismic studies to derive M_w potentials for active faults, particularly in areas where natural and/or anthropogenic surface processes have reduced or obscured the geomorphic expression of past surface-rupturing earthquakes. The broadly distributed nature of GF deformation at several locations, together with fault scarp heights less than or equal to heights of the fluvial bars, channels, and dunes comprising the faulted Late Pleistocene surface, suggests that large stretches of the GF rupture will be challenging to recognize in as little as 10^1–10^3 yr. This has implications for future seismic-hazard assessment in the Canterbury Plains region and the search for possible prehistoric GF-type ruptures elsewhere. The involvement of additional fault ruptures that contributed to the Darfield earthquake moment release (Gledhill et al., 2011; Beavan et al., 2010) provides additional challenges as these faults did not leave easily identifiable surface manifestations. Recent catastrophic earthquakes involving complex ruptures on previously unidentified "blind" sources (e.g., Hayes et al., 2010) highlight the need for combining subsurface investigations with traditional paleoseismic techniques in seismic-hazard analysis.

Seismologically derived $\Delta\sigma$ values for large earthquakes generally vary from 1 to 10 MPa, with higher $\Delta\sigma$ attributed to longer earthquake recurrence intervals that allow more time for fault annealing (Kanamori, 1994). This relationship is supported by relatively high geodetically derived $\Delta\sigma$ for the M_w 7.3 Landers (8 ± 1 MPa) and M_w 7.1 Hector Mine (10 ± 2 MPa) earthquakes (Price and Bürgmann, 2002) on faults with likely earthquake recurrence intervals of 5–15 k.y. (Rockwell et al., 2000). We attribute the relatively high GF $\Delta\sigma^G$ of 13.9 ± 3.7 MPa to the rupture of a "strong fault" with an earthquake recurrence interval of sufficient duration to allow significant interseismic annealing. As is evident from both the 1992 Landers and 2010–2011 Canterbury earthquake sequences, regions of relatively low strain rates and "strong" faults within active plate boundary zones are susceptible to earthquake clustering, complex fault arrays, and high-$\Delta\sigma$ ruptures. The Canterbury earthquake sequence highlights the devastating potential of these sequences if they occur in close proximity to major urban centers.

ACKNOWLEDGMENTS

We thank R. Jongens, D. Townsend, J. Begg, W. Ries, J. Claridge, A. Klahn, H. Mackenzie, A. Smith, S. Hornblow, R. Nicol, S. Cox, R. Langridge, and K. Pedley for assistance with fault rupture mapping. D. Rhoades is thanked for D_{avg} modeling. Landowners are gratefully acknowledged. LiDAR images are courtesy of ECan and NZ Aerial Mapping Limited. We thank M. Hemphill-Haley, R. Norris, J. Pettinga, G. de Pascale, and two anonymous reviewers for constructive comments on this manuscript.

REFERENCES CITED

Beavan, J., Samsonov, S., Motagh, M., Wallace, L., Ellis, S., and Palmer, N., 2010, The M_w 7.1 Darfield (Canterbury) earthquake: Geodetic observations and preliminary source model: Bulletin of the New Zealand Society for Earthquake Engineering, v. 43, p. 228–235.

Berryman, K., Webb, T., Hill, N., Stirling, M., Rhoades, D., Beavan, J., and Darby, D., 2002, Seismic loads on dams, Waitaki system, earthquake source characterisation: GNS client report 2011/129, 80 p.

Clark, M.M., 1972, Surface rupture along the Coyote Creek fault: U.S. Geological Survey Professional Paper 787, p. 55–87.

DeMets, C., Gordon, R.G., and Argus, D.F., 2010, Geologically current plate motions: Geophysical Journal International, v. 181, p. 1–80, doi:10.1111/j.1365-246X.2009.04491.x.

Forsyth, P.J., Barrell, D.J.A., and Jongens, R., 2008, Geology of the Christchurch area: Institute of Geological and Nuclear Sciences Geological Map 16, scale 1:250,000, 1 sheet, 67 p. text.

Gledhill, K., Ristau, J., Reyners, M., Fry, B., and Holden, C., 2011, The Darfield (Canterbury, New Zealand) M_w 7.1 earthquake of September 2010: A preliminary seismological report: Seismological Research Letters, v. 82, p. 378–386, doi:10.1785/gssrl.82.3.378.

Griffith, W., Di Toro, G., Pennacchioni, G., Pollard, D., and Nielsen, S., 2009, Static stress drop associated with brittle slip events on exhumed faults: Journal of Geophysical Research, v. 114, B02402, doi:10.1029/2008JB005879.

Hanks, T.C., and Kanamori, H., 1979, A moment magnitude scale: Journal of Geophysical Research, v. 84, p. 2348–2350, doi:10.1029/JB084iB05p02348.

Hayes, G.P., Briggs, R.W., Sladen, A., Fielding, E.J., Prentice, C., Hudnut, K., Mann, P., Taylor, F.W., Crone, A.J., Gold, R., Ito, T., and Simons, M., 2010, Complex rupture during the 12 January 2010 Haiti earthquake: Nature Geoscience, v. 3, p. 800–805, doi:10.1038/ngeo977.

Holden, C., Beavan, J., Fry, B., Reyners, M., Ristau, J., Van Dissen, R., Villamor, P., and Quigley, M., 2011, Preliminary source model of the M_w 7.1 Darfield earthquake from geological, geodetic and seismic data: Proceedings of the Ninth Pacific Conference on Earthquake Engineering, Building an Earthquake-Resilient Society, 14–16 April 2011, Auckland, New Zealand, Paper 164, 7 p.

Jongens, R., Pettinga, J., and Campbell, J., 1999, Stratigraphic and structural overview of the onshore Canterbury Basin: North Canterbury to the Rangitata River: Report prepared for Indo-Pacific Energy Ltd. Permit PEP38256, University of Canterbury, 31 p.

Kanamori, H., 1994, Mechanics of earthquakes: Annual Review of Earth and Planetary Sciences, v. 22, p. 207–237, doi:10.1146/annurev.ea.22.050194.001231.

Madariaga, R., 1977, Implications of stress-drop models of earthquakes for the inversion of stress drop from seismic observations: Pure and Applied Geophysics, v. 115, p. 301–316, doi:10.1007/BF01637111.

Pettinga, J.R., Yetton, M.D., Van Dissen, R.J., and Downes, G., 2001, Earthquake source identification and characterisation for the Canterbury region, South Island, New Zealand: Bulletin of the New Zealand Society for Earthquake Engineering, v. 34, p. 282–315.

Prentice, C., Mann, P., Crone, A.J., Gold, R., Hudnut, K., Briggs, R., Koehler, R., and Jean, P., 2010, Seismic hazard of the Enriquillo–Plantain Garden fault in Haiti inferred from palaeoseismology: Nature Geoscience, v. 3, p. 789–793, doi:10.1038/ngeo991.

Price, E., and Bürgmann, R., 2002, Interactions between the Landers and Hector Mine, California, earthquakes from space geodesy, boundary element modeling, and time-dependent friction: Bulletin of the Seismological Society of America, v. 92, p. 1450–1469, doi:10.1785/0120000924.

Quigley, M., and 22 others, 2010, Surface rupture of the Greendale fault during the M_w 7.1 Darfield (Canterbury) earthquake, New Zealand: Initial findings: Bulletin of the New Zealand Society for Earthquake Engineering, v. 43, p. 236–242.

Rockwell, T., Lindvall, S., Herzberg, M., Murbach, D., Dawson, T., and Berger, G., 2000, Paleoseismology of the Johnson Valley, Kickapoo, and Homestead Valley faults: Clustering of earthquakes in the eastern California shear zone: Bulletin of the Seismological Society of America, v. 90, p. 1200–1236, doi:10.1785/0119990023.

Sibson, R., Ghisetti, F., and Crookbain, R., 2011, 'Andersonian' wrench faulting in a regional stress field during the 2010–2011 Canterbury, New Zealand, earthquake sequence, *in* Healey, D., ed., Faulting, fracturing and igneous intrusion in the Earth's crust: The Geological Society of London Special Publication (in press).

Terres, R.R., and Sylvester, A.G., 1981, Kinematic analysis of rotated fractures and blocks in simple shear: Bulletin of the Seismological Society of America, v. 71, p. 1593–1605.

Trifunac, M.D., and Brune, J.N., 1970, Complexity of energy release during the Imperial Valley, California, earthquake of 1940: Bulletin of the Seismological Society of America, v. 60, p. 137–160.

Wallace, L.M., Beavan, R.J., McCaffrey, R., Berryman, K.R., and Denys, P., 2007, Balancing the plate motion budget in the South Island, New Zealand using GPS, geological and seismological data: Geophysical Journal International, v. 168, p. 332–352, doi:10.1111/j.1365-246X.2006.03183.x.

Wells, D.L., and Coppersmith, K.J., 1994, New empirical relationships among magnitude, rupture length, rupture width, rupture area, and surface displacement: Bulletin of the Seismological Society of America, v. 84, p. 974–1002.

Wesnousky, S.G., 2008, Displacement and geometrical characteristics of earthquake surface ruptures: Issues and implications for seismic-hazard analysis and the process of earthquake rupture: Bulletin of the Seismological Society of America, v. 98, p. 1609–1632, doi:10.1785/0120070111.

Manuscript received 3 June 2011
Revised manuscript received 6 August 2011
Manuscript accepted 24 August 2011

Printed in USA